

Hyperspectral holographic Fourier-microscopy

G.S. Kalenkov, S.G. Kalenkov, A.E. Shtan'ko

Abstract. A detailed theory of the method of holographic recording of hyperspectral wave fields is developed. New experimentally obtained hyperspectral holographic images of microscopic objects are presented. The possibilities of the method are demonstrated experimentally using the examples of urgent microscopy problems: speckle noise suppression, obtaining hyperspectral image of a microscopic object, as well as synthesis of a colour image and obtaining an optical profile of a phase object.

Keywords: Fourier-microscopy, holographic images, hyperspectral wave fields.

1. Introduction

In this paper we consider a new application of a Fourier spectrometer, namely the hyperspectral recording of holograms of microscopic objects in noncoherent light. Fourier spectroscopy represents undoubtedly one of the first examples of successful application of computers in optics. As is well known [1], the spectral composition of radiation carrying information about optical properties of a sample is determined by the numerical Fourier transform of the interferogram obtained at the interferometer output in the process of varying the length of one of its arms. Two types of interferograms are distinguished: symmetrical and asymmetrical. Symmetrical interferograms are obtained when a sample is placed in the superimposed beams behind a beam splitter. In this case, the Fourier transform of the interferogram provides information about the energy spectrum of radiation, i.e. modulus of the spectral density amplitude of radiation transmitted through the sample. Of particular interest is certainly an asymmetric interferogram that is obtained when a sample is positioned in one of the interferometer arms (in place of a fixed mirror). In this case, the Fourier transform of the interferogram yields a complex amplitude of the spectrum of radiation reflected from the sample, the amplitude containing complete information about the spectral properties of the sample, namely, the

dependences of the complex refractive index of the sample on the spectral frequency $\sigma = \lambda^{-1}$ (λ is the wavelength).

Formally, the optical scheme of asymmetric interferogram registration coincides with the scheme of hologram recording. Indeed, in both cases an interfering object and reference light beams are present. However, in the Fourier spectrometer, the interferogram is recorded by a point-like detector, while in the holographic scheme, a digital hologram (or an interferogram) is recorded with a digital camera as a two-dimensional field intensity in some plane.

Now, if a digital camera is installed instead of a point-like receiver, and a micro-object is used as a sample, the object light beam will illuminate the entire matrix aperture as a result of diffraction. The interference of the object light beam with the reference beam during the reference mirror motion allows writing the interferogram into each matrix pixel. We have shown that the Fourier transform of these interferograms determines the complex amplitude of the object's diffracted field for each spectral radiation frequency, i.e. the hyperspectral hologram. The following important fact should be noted here: the parameters of modern digital matrices allow their successful use for recording the diffraction patterns of micro-objects [2].

By solving the inverse diffraction problem with the use of the Fourier or Fresnel transforms, we obtain a complex transmittance function of the micro-object at an arbitrary spectral frequency. Thus, the Fourier spectrometer represents not only a spectral device, i.e. an instrument capable of determining the transmittance or absorption spectra of samples with very high resolution, but also a device that, as it turns out, can do much more: it can record digital hyperspectral holograms of the micro-objects under polychromatic radiation. We have shown the principal possibility of such a recording in [3–5]. In [6], we have developed a theory of the proposed method and obtained experimentally hyperspectral holograms of the samples of some micro-objects. In this paper, we present the results of new theoretical and experimental studies on hyperspectral Fourier-holography of microscopic objects.

2. Model

Let the object positioned in one of the arms of a Michelson interferometer in place of a fixed mirror be illuminated by a polychromatic wave. Similar to [1], we represent the complex amplitude of the polychromatic field in the form

$$u = \int_{\Omega} E(\sigma) \exp(2\pi i \sigma z) d\sigma,$$

where z is the coordinate; $E(\sigma)$ is the spectral density function of the amplitude, which is assumed known; and Ω is the value

G.S. Kalenkov Moscow Institute of Physics and Technology (State University), Institutskii per. 9, 141700 Dolgoprudnyi, Moscow region, Russia, e-mail: kalenkov@mail.ru;

S.G. Kalenkov Moscow State University of Mechanical Engineering, Bol'shaya Semenovskaya ul. 38, 107023 Moscow, Russia, e-mail: kaser45@gmail.com;

A.E. Shtan'ko Moscow State University of Technology 'Stankin' (MSTU 'Stankin'), Vadkovskii per. 3a, 127055 Moscow, Russia, e-mail: valdaisky@gmail.com

Received 16 June 2014; revision received 23 August 2014
Kvantovaya Elektronika 45 (4) 333–338 (2015)
Translated by M.A. Monastyrskiy

of a spectral window of illuminating radiation, i.e. the spectral region in which the function $E(\sigma)$ is different from zero. Without loss of generality, we will consider below the transmitting transparency. Let $a(\sigma, \mathbf{x}) = |a(\sigma, \mathbf{x})| \exp[i\varphi(\sigma, \mathbf{x})]$ be a complex transmittance function of the object-transparency at some specific frequency σ , where $\varphi(\sigma, \mathbf{x}) = \arctan[\text{Im} a(\sigma, \mathbf{x}) / \text{Re} a(\sigma, \mathbf{x})]$ is the wave field phase, and \mathbf{x} is a two-dimensional coordinate of the object in the plane $z = 0$. Consider a single spectral component of the plane light wave $E(\sigma) \exp(2\pi i \sigma z)$. The transparency action on this component is reduced to the multiplication by a complex transmittance function, so that, after the passage of this spectral component through the transparency, the wave field at the object-transparency output, associated with that component, appears as

$$u_\sigma(\mathbf{x}) = a(\sigma, \mathbf{x}) E(\sigma) \exp(2\pi i \sigma z) \Big|_{z=0} = a(\sigma, \mathbf{x}) E(\sigma).$$

The above considerations can be generalised to the case of an arbitrary hyperspectral object. We consider the hyperspectral object as the object-transparency, which affects each monochromatic component of the incident field, so that the wave field at the transparency output can be represented as

$$\begin{aligned} u_\Omega(\mathbf{x}) &= \int_\Omega a(\sigma, \mathbf{x}) E(\sigma) \exp(2\pi i \sigma z) \Big|_{z=0} d\sigma \\ &= \int_\Omega a(\sigma, \mathbf{x}) E(\sigma) d\sigma. \end{aligned} \quad (1)$$

The hyperspectral transparency action on polychromatic radiation is determined by optical properties of the object-transparency material, and in particular, by spatial distribution of the complex refractive index.

We assume below that the region $\Omega = \sigma_{\max} - \sigma_{\min}$ coincides with the characteristic width of transmittance function's spectral window of the hyperspectral object-transparency. In the general case, the complex wave field $a(\sigma, \mathbf{x})$ of the object is associated with the complex amplitude $A(\sigma, \xi)$ of the diffraction field in the recording plane by means of the integral transformation $A(\sigma, \xi) = \Phi_\sigma(a(\sigma, \mathbf{x}))$, where ξ is a two-dimensional coordinate in the recording plane. The form of the integral transform Φ_σ and, consequently, of the diffraction field depends on the geometry of the problem: in particular, the integral operator Φ_σ may signify the Fourier transform as in our paper [5], and the Fresnel transform in a more general case:

$$A(\sigma, \xi) = \Phi_\sigma(a(\sigma, \mathbf{x})) = \int_d a(\sigma, \mathbf{x}) \exp\left[\pi i \sigma \frac{(\mathbf{x} - \xi)^2}{z}\right] d\mathbf{x}. \quad (2)$$

Assume that the object size d and the distance z from the object to the recording plane obey the Fresnel diffraction conditions. Then, the complex amplitude $U(\sigma, \xi)$ of the object wave on the spectral component σ in the matrix plane is $U(\sigma, \xi) = \exp(2\pi i \sigma z) E(\sigma) A(\sigma, \xi)$. (The exponential factor $\exp(2\pi i \sigma z)$ describes the linear phase incursion when the wave propagates from the transparency to the matrix.) The total complex amplitude $U_\Omega(\xi)$ of the polychromatic diffraction field in the recording plane has the form

$$U_\Omega(\xi) = \int_\Omega U(\sigma, \xi) d\sigma = \int_\Omega \exp(2\pi i \sigma z) E(\sigma) A(\sigma, \xi) d\sigma. \quad (3)$$

Only spectral components having the same frequency σ undergo interference; therefore, the spectral density of the interference field intensity is associated with the object wave

$U_G(\xi)$ and the reference wave $E(\sigma) \exp[2\pi i \sigma(z + \delta)]$ reflected from the movable mirror that is shifted by the distance δ from the position of the zero path difference $I(\sigma, \xi, \delta) = S(\sigma) |A(\sigma, \xi) + \exp(2\pi i \sigma \delta)|^2$, where $S(\sigma) = |E(\sigma)|^2$ is the source power density at the spectral frequency. Of course, the total intensity $G(\xi, \delta)$, i.e. the integral of the function $I(\sigma, \xi, \delta)$ over all spectral frequencies: $G(\xi, \delta) = \int_\Omega I(\sigma, \xi, \delta) d\sigma$ is recorded in each pixel of the matrix. In this integral, of interest is only the interference term

$$\begin{aligned} G(\xi, \delta) &= \int_\Omega S(\sigma) [A(\sigma, \xi) \exp(-2\pi i \sigma \delta) \\ &\quad + A^*(\sigma, \xi) \exp(2\pi i \sigma \delta)] d\sigma. \end{aligned} \quad (4)$$

Expression (4) for $G(\xi, \delta)$, as a function of the mirror displacement δ , represents a spatial-spectral interferogram of the object since it depends both on the spatial coordinate ξ of the object field in the matrix plane and on the spectral properties of the object itself, which are characterised by the object transmittance function $a(\sigma, \mathbf{x})$. It is assumed that the spectral composition $S(\sigma)$ of the light source is known. Note that expression (4) coincides with the corresponding formulas in Fourier spectrometry for the case when the sample is installed in one of the arms of an asymmetric interferometer [1]. The derivation of (4) assumes implicitly that the light beam illuminating the object has a high spatial coherence that is virtually equal to unity. By performing the Fourier transform of the interferogram $G(\xi, \delta)$ and taking into account the fact that $S(-\sigma) = 0$ for the negative frequency spectrum, we obtain from (4) the expression for the complex amplitude of the diffraction field:

$$A(\sigma, \xi) = \frac{\int G(\xi, \delta) \exp(2\pi i \sigma \delta) d\delta}{S(\sigma)}. \quad (5)$$

Thus, knowing the spectral composition of the light source, i.e. the function $S(\sigma)$ and the interferogram $G(\xi, \delta)$ at each point ξ of the matrix, it is possible, using the inverse transform Φ_σ^{-1} of the function $A(\sigma, \xi)$, to obtain a holographic image of the object for each spectral frequency σ .

Let us now discuss formula (5). Of course, the exact Fourier transform of the interferogram $G(\xi, \delta)$ according to formula (5) is only possible under the condition that integral (5) is taken in infinite limits. In reality, the mirror displacement δ is limited to the mirror stroke length L , i.e. to the magnitude of the interval $-L \leq \delta \leq L$.

This circumstance imposes a natural limitation on the spectral resolution of the complex amplitude $A(\sigma, \xi)$ of the diffraction field itself. Indeed, suppose for simplicity that there is a 'two-colour' object-transparency in the plane \mathbf{x} , whose action on the polychromatic wave field (1) is that it only transmits two monochromatic components $E(\sigma_1)$ and $E(\sigma_2)$, while the rest components are either reflected or absorbed. Such an object can be formally represented as two different objects: $a_1 = a(\sigma_1, \mathbf{x})$ and $a_2 = a(\sigma_2, \mathbf{x})$. According to formula (2), these objects correspond to two diffraction fields $A_1 = A(\sigma_1, \xi)$ and $A_2 = A(\sigma_2, \xi)$, respectively. Obviously, the fields A_1 and A_2 are spectrally resolvable in each pixel of the matrix, and therefore those fields are spatially distinguishable provided that the mirror stroke length $L \geq \Delta\sigma^{-1} = (\sigma_2 - \sigma_1)^{-1}$. Under this condition, by performing the inverse Fresnel transform (2), we can reconstruct the objects a_1 and a_2 .

Let us now consider a multispectral object. We divide the spectral region of the multispectral object-transparency into

$M = \Omega/\Delta\sigma = \Omega L$ intervals. Then, according to formula (5), provided that the mirror stroke length L is given, we can calculate M spatial-spectral components $A_m = A(\sigma_m, \xi)$, $m = 1, 2, \dots, M$, which then give a set of M complex functions $a_m = a(\sigma_m, \mathbf{x})$, $m = 1, 2, \dots, M$, representing a set of reconstructed holographic images of the object. According to (1), the sum

$$u_\Omega(x) = \Delta\sigma \sum_1^M a(\sigma_m, \mathbf{x}) E(\sigma_m) = \frac{1}{L} \sum_1^M a(\sigma_m, \mathbf{x}) E(\sigma_m) \quad (6)$$

over such a set represents a reconstructed wave field of the hyperspectral object.

It is well known (see, for example, [1]) that the advantage of a Fourier spectrometer and its high resolving power compared to diffraction instruments actually stem from two main components known as Jacquinot's (throughput) and Felgett's advantage (multiplex). In our case, the advantage in multiplexing is conditioned by the fact that during the entire time of exposure or recording the interferogram $G(\xi, \delta)$, the Fourier spectrometer matrix simultaneously records all the spectral components $A_m = A(\sigma_m, \xi)$ of the object. The number M of these components is equal to the multiplex. In comparison with recording of hyperspectral holograms using, for example, a tunable laser, this implies that in our case we obtain a significant advantage in the signal-to-noise ratio. As is known from Fourier spectroscopy theory, this advantage is proportional to \sqrt{M} . In our experiments described below, the value of M is about 500, and so the signal-to-noise ratio is twenty times higher. Another important advantage of Fourier spectroscopy, associated with increasing signal-to-noise ratio and, as a consequence, with increasing resolution, is the possibility of multiple scanning. It leads to averaging of noise in recording of all spectral components $A_m = A(\sigma_m, \xi)$ and to lowering of the noise average level, which, obviously, enhances the spatial-spectral resolution of the reconstructed holographic images of microscopic objects.

Consider now the procedure of reconstructing the hyperspectral holographic images, based on formula (5).

As noted above, the complex amplitude of the diffraction field in the matrix plane and the object field are related by the Fresnel transform (2). Let us represent this transform in more detail:

$$A(\sigma, \xi) = \exp\left(2\pi i \sigma \frac{\xi^2}{2z}\right) \times \int_d a(\sigma, \mathbf{x}) \exp\left(2\pi i \sigma \frac{\mathbf{x}^2}{2z}\right) \exp(-2\pi i \sigma \theta \mathbf{x}) d\mathbf{x}. \quad (7)$$

The expression

$$A_F(\sigma \xi/z) = \int_D a(\sigma, \mathbf{x}) \exp(-2\pi i \sigma \mathbf{x} \xi/z) d\mathbf{x} \quad (8)$$

is an exact Fourier-image of the object field $a(\sigma, \mathbf{x})$ at the spectral frequency σ (D is the matrix size). In order to determine the complex amplitude of the object field $a(\sigma, \mathbf{x})$, we multiply (7) by the conjugate factor $\exp(-2\pi i \sigma \xi^2/2z)$ that stands in front of the integral, and then perform the inverse Fourier transform. As a result, we obtain

$$a(\sigma, \mathbf{x}) \exp\left(2\pi i \sigma \frac{\mathbf{x}^2}{2z}\right) = F^{-1} \left[A(\sigma, \xi) \exp\left(-2\pi i \sigma \frac{\xi^2}{2z}\right) \right], \quad (9)$$

where F^{-1} is the inverse Fourier transform operator. Multiplying (9) by the conjugate factor $\exp(-2\pi i \sigma \mathbf{x}^2/2z)$, we finally obtain

$$a(\sigma, \mathbf{x}) = \exp\left(-2\pi i \sigma \frac{\mathbf{x}^2}{2z}\right) F^{-1} \left[A(\sigma, \xi) \exp\left(-2\pi i \sigma \frac{\xi^2}{2z}\right) \right]. \quad (10)$$

Note that there is a certain difficulty: the distance z between the object plane and matrix is only known with a certain accuracy $\Delta z \ll z$. To determine $a(\sigma, \mathbf{x})$ from expression (10), we need to define accurately the value of z , or, figuratively speaking, we need to 'focus' accurately enough. Let us estimate the focusing accuracy required, i.e. the ratio $\Delta z/z$. Suppose, an approximate value $z + \Delta z$ has been used instead of the exact value of z in the quadratic factor $\exp(-2\pi i \sigma \xi^2/2z)$. Obviously, the phase error caused by the focusing inaccuracy is determined by the factor $\exp[\pi i \sigma (\xi^2/z)(\Delta z/z)]$. The focusing accuracy can be considered acceptable if this factor is approximately equal to unity, which leads to a chain of inequalities:

$$\pi \sigma \frac{\xi^2}{z} \frac{\Delta z}{z} \ll \pi, \text{ or } \sigma \frac{D^2}{z} \frac{\Delta z}{z} \ll 1, \text{ or } \Delta z \ll \frac{\lambda z^2}{D^2} = \lambda \theta_0^2, \quad (11)$$

where D is the matrix size and $\theta_0 = D/z$. Note that the latter inequality in (11) coincides with the known expression for the depth of field Δz of an objective with the numerical aperture $\theta_0 = D_{\text{ob}}/z$, where D_{ob} is the aperture size of the objective with the focal length $f = z$.

3. Experiment

Figure 1a shows a schematic layout of the holographic optical Fourier spectrometer. As a polychromatic radiation source (I), we used a fibre laser emitting a supercontinuum of 200 mW in the wavelength range from 0.45 to 2 μm . Radiation from source (I) is split by a beam-splitting cube (2) and prism (3), and then directed to object (4) and matrix (8). The prism (6) mounted on a piezo table (7) directs the reference wave to the matrix through the beam-splitting cube (5). Stepwise displacement of the table (step $\delta = 0.1 \mu\text{m}$, stroke length $L = 100 \mu\text{m}$) is synchronised [unit (9)] with interferogram recording on the matrix (8). The recording rate is 10 frames per second, the total number of interferograms is 1000 for a single scanning, and the frame format of the CMOS-sensor is 1024×1024 pixels, 10 bits per pixel.

The algorithm of digital processing of interferograms and forming the micro-object image is shown schematically in Figure 1b. In accordance with (5), we calculated a set of holo-

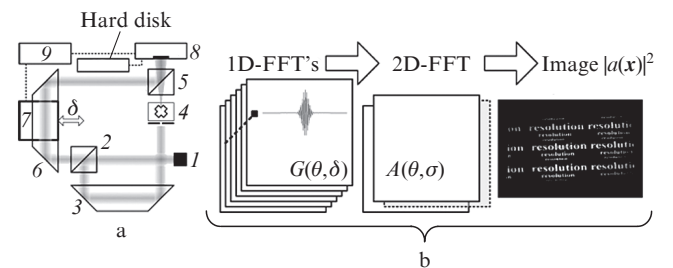


Figure 1. (a) Principal optical scheme of an optical holographic Fourier spectrometer and (b) scheme of digital processing of interferograms and imaging of a micro-object; (1D-FFT) one-dimensional and (2D-FFT) two-dimensional Fast Fourier transforms.

grams of the micro-object diffraction field, which requires calculation of a one-dimensional Fourier transform by the variable δ for each pixel in the array of interferograms. In accordance with (10), the inverse Fresnel transform was used to determine the object field complex amplitude $a(\sigma, \mathbf{x})$. The spatial intensity distribution of square modulus of the object field's complex amplitude $|a(\sigma, \mathbf{x})|^2$ represents an amplitude image of the micro-object, while the expression $\arctan[\text{Im}a(\sigma, \mathbf{x})/\text{Re}a(\sigma, \mathbf{x})]$ gives a phase image of the micro-object at a selected spectral frequency σ . Below, we call the amplitude and phase images at the frequency σ the monochromatic images. In accordance with (6), the sum of monochromatic images represents a hyperspectral image of the object.

It is important to note that the thus obtained hyperspectral image possesses the property of exact physical colour rendering. This is confirmed by our experiments. Figure 2 illustrates a process of synthesising the colour image. A cut of the lotus stem illuminated through the frosted glass was used as an object.

The spectral range from 0.45 to 0.7 μm comprises 145 spatial-spectral components, and for each of them we obtained a monochromatic image A_m in grey gradations. After that, each monochromatic image was 'painted' in its own colour according to the CIE 1931 colour space. Figures 2a–e represent the coloured monochromatic images for some wavelengths. A sum of all 145 coloured monochromatic images gives a coloured hyperspectral image of the micro-object (Fig. 2f). Figures 2g and 2h show the central areas of the object image obtained with a conventional microscope at the magnification of $\sim 100\times$ and with our setup, respectively. A good agreement of colour of the synthesised image and original image was obtained.

Summation of monochromatic images leads to the speckle-noise suppression, which is present in each of the monochromatic images if the object possesses the property of diffuse light scattering. Random modulation of the phase wave in the scattering medium depends not only on the inhomogeneity of the medium, but also on the radiation wavelength. Therefore, the monochromatic images for different wavelengths have different speckle-structures, which stipulates the possibility of their averaging in the summation of

monochromatic images. The effect of speckle-noise suppression is demonstrated in an experiment with illumination of an object (the ant's head) through frosted glass installed under the mask (4) of 1 mm in size, which ensures diaphragming of the object (Fig. 1a). Figure 3a shows a monochromatic image for $\lambda = 0.5 \mu\text{m}$, in which the speckle-structure that is caused by diffuse scattering and makes it difficult to observe fine details is clearly visible. As in the previous experiment, we obtained 145 monochromatic images and synthesised a hyperspectral image (Fig. 3b), for which the speckle-structure contrast was significantly reduced. It may be noted that unlike some approaches that have been proposed to diminish the speckle noise [7–10], this method does not lead to a decrease in spatial resolution.

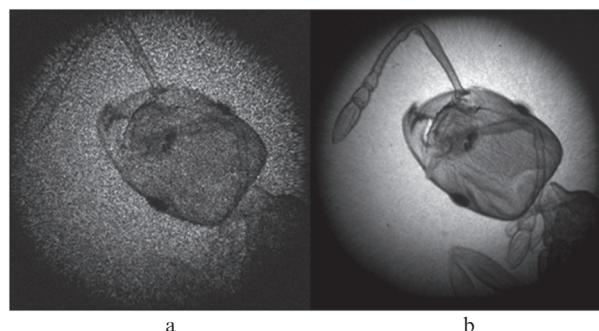


Figure 3. Image of the ant's head reconstructed for (a) a single spectral component and (b) a sum of 145 spectral components.

Our method of hyperspectral Fourier holographic microscopy allows focusing on different planes of a three-dimensional object. Expressions (11) determine the depth of field and focusing accuracy. That possibility is illustrated in our experiments on the recording of a two-layer object representing two superimposed standard ocular scales illuminated through the frosted glass. The longitudinal distance between the scales is 2 mm. The hyperspectral images of both scales, calculated at two different focus settings z , are shown in Fig. 4. It can be seen that the overlap of images is absent.

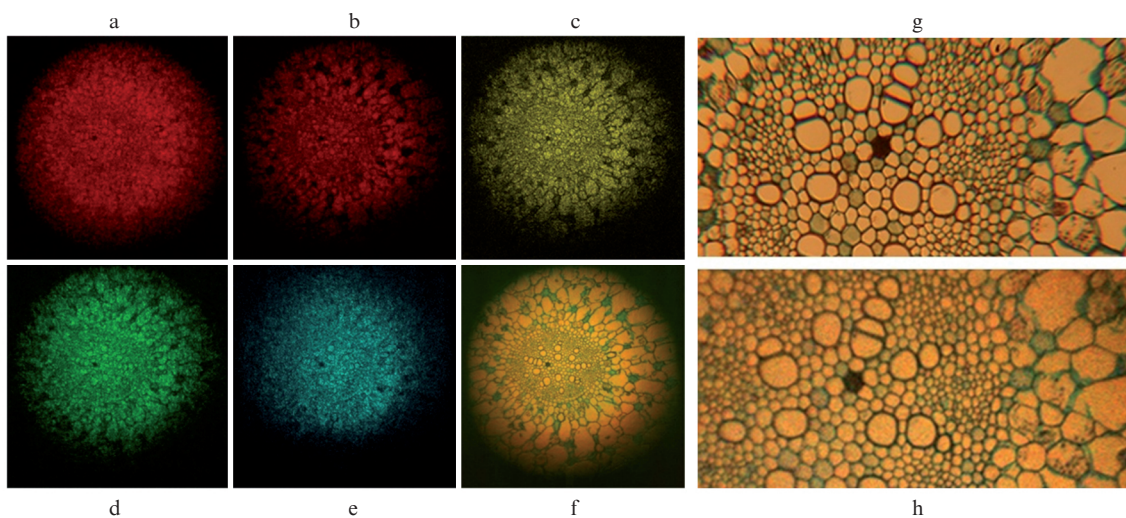


Figure 2. (Colour online) Synthesis of a colour image: (a–e) monochromatic images, (f) total colour image, (h) its fragment and (g) the same fragment observed with an optical microscope.

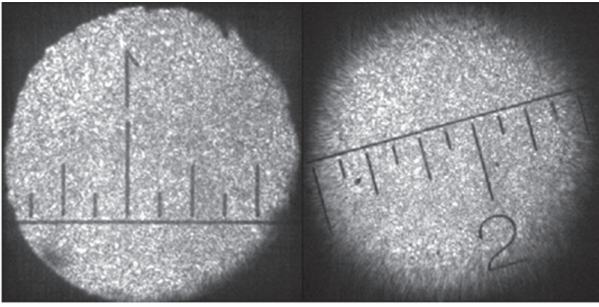


Figure 4. Digital focusing of two ocular scales on different planes.

Hyperspectral holographic Fourier microscopy provides additional opportunities in observation of phase objects. Visualisation of phase objects was first implemented in 1930 by Zernike who proposed the phase-contrast method. As is well known, this method allows visualisation of transparent phase objects with small phase variation. Hyperspectral holographic Fourier microscopy allows calculating the phase $\varphi(\sigma, \mathbf{x})$ of the object wave field for any spectral frequency. This function provides information about the optical thickness (optical profile) of the object and in many cases is more informative than a usual amplitude image. The opportunity of reconstructing the polychromatic wave field allows implementation of a new way of representing the information about the object's optical thickness in the form of an integral optical profile. We are talking here about the superposition of the phase images obtained for different spectral components. However, their direct summation is incorrect since the phase shift $\varphi = 2\pi\sigma n\Delta z$ depends on the spectral frequency σ , object thickness Δz and refractive index n . If the light dispersion is neglected, the optical thickness $n\Delta z = \varphi/2\pi\sigma$ of the object does not depend on the wavelength, and we call this value the optical profile of the object. By averaging the optical profiles of all spectral components, we obtain the integral optical profile, in which the noises inherent in individual components are smoothed. Figure 5 demonstrates an example of the integral profile of a cut of the earthworm, constructed by means of this approach.

The similarity of the optical profile image for a single spectral component (Fig. 5a) and the phase image obtained by the digital holographic microscopy in coherent radiation consists in the fact that these images contain a coherent speckle-noise typical of a scattering object. Figures 5b and 5c clearly demonstrate an increase in quality of the optical pro-

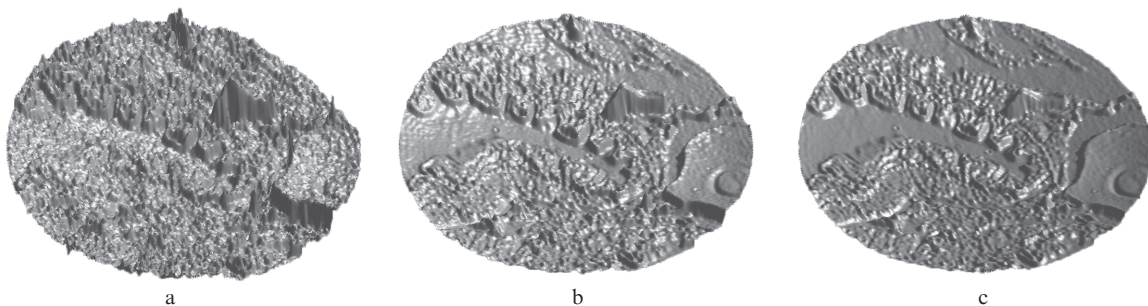


Figure 5. Image of the optical profile of the earthworm cut constructed for (a) a single spectral component, as well as the integral profile constructed for (b) 25 and (c) 50 spectral components.

file image with increasing number of spectral components involved in calculations.

Figure 6 shows an image of the standard test pattern No. 1 for a wavelength of $1 \mu\text{m}$ and an image fragment for a wavelength of $0.45 \mu\text{m}$. We can observe a decrease in the contrast of strokes with increasing spatial frequency. This occurs due to the limited numerical aperture of the record, which in our case was about 0.2. The diffraction limit of resolution at such an aperture is $6.1 \mu\text{m}$ for the wavelength $\lambda = 1 \mu\text{m}$ and $2.75 \mu\text{m}$ for $\lambda = 0.45 \mu\text{m}$. The width of the smallest resolvable strokes of the 10th square is $5.9 \mu\text{m}$, and that of the 21st square – $3 \mu\text{m}$. Thus, the experimental results are consistent with theoretical evaluation of the diffraction limit of resolution.

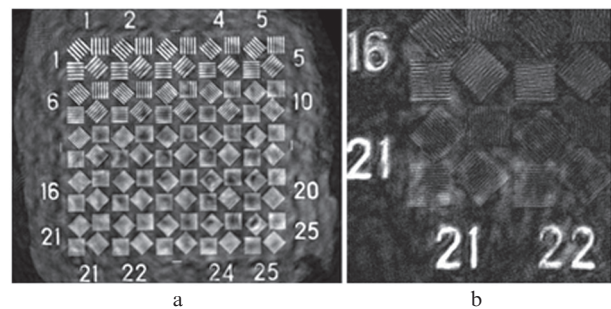


Figure 6. (a) Image of the standard test pattern No. 1 for $\lambda = 1 \mu\text{m}$ and (b) its fragment for $\lambda = 0.45 \mu\text{m}$.

Obviously, the proposed method requires considerable processing resources. A single series of interferograms involves a memory of $1024 \times 1024 \times 1000 \times 10 \text{ bit} = 1.25 \text{ GB}$. The Fourier transform requires twice as much memory space, i.e. 2.5 GB . Due to the fast-Fourier transform symmetry, only half of the data is used. Since the interferograms in each pixel are processed independently, they can be loaded from the hard disk and processed successively. However, this approach to the calculation is rather time-consuming.

4. Conclusions

The method of hyperspectral holographic Fourier microscopy we have proposed is based on the possibility of recording the holograms in hyperspectral incoherent radiation. In our opinion, this opens up a way to urgent and important practical applications of this method, for example, in study-

ing the objects in the terahertz or X-ray range. Within those ranges, we face a lack of sufficiently cheap and available sources of coherent radiation. However, the modern level of means for radiation recording gives reason to hope that our method will be promising for obtaining hyperspectral holograms in these spectral ranges. Since the method is based on the principles and techniques of Fourier spectroscopy, it naturally inherits all the advantages of these principles: unprecedentedly high signal-to-noise ratio and, consequently, high spatial-spectral resolution of the holographic image in comparison, for example, with the hyperspectral holograms obtained by a tunable laser. Finally, we emphasize the most significant advantage of hyperspectral Fourier-holography: the method allows one to detect the amplitude, phase and frequency of the field within a single recording process, which gives actual grounds to call it holography, i.e. a 'full record'.

Acknowledgements. The authors are grateful to A.V. Masalov and A.V. Kraiskiy for their interest in this work and constructive discussions. This work was supported by the Russian Foundation for Basic Research (Grant Nos 13-07-00473 and 14-07-00873).

References

1. Bell R.J. *Introductory Fourier Transform Spectroscopy* (New York: Academic Press, 1972; Moscow: Mir, 1975).
2. Vlasov N.G., Kalenkov S.G., Krilov D.V., Stanko A.E. *Proc. SPIE Int. Soc. Opt. Eng.*, **5821**, 158 (2005).
3. Kalenkov S.G., Kalenkov G.S., Shtan'ko A.E. *Izm. Tekh.*, **11**, 21 (2012).
4. Kalenkov S.G., Kalenkov G.S., Shtan'ko A.E. *Radiotekh. Elektron.*, **58** (12), 1 (2013).
5. Kalenkov S.G., Lokshin G.R. *Radiotekh. Elektron.*, **58** (3), 247 (2013).
6. Kalenkov S.G., Kalenkov G.S., Shtanko A.E. *Opt. Express*, **21** (21), 24985 (2013).
7. Maycock J., Hennelly B.M., McDonald J.B. *J. Opt. Soc. Am. A*, **24** (6), 1617 (2007).
8. Desjardins A.E., Vakoc B.J., Oh W.Y., Motaghianezam S.M.R. *Opt. Express*, **15** (10), 6200 (2007).
9. Pan F., Xiao W., Liu S., Wang F., Rong L., Li R. *Opt. Express*, **19** (5), 3862 (2011).
10. Shtan'ko A.E., Kalenkov G.S., Ivanov S.D., Kalutskov O.A. *Izm. Tekh.*, **11**, 23 (2013).